Duality between Creep and Relaxation of a Cement Paste at Different Levels of Relative Humidity: Characterization by Microindentation and Analytical Modeling

Zhao Chen, Luca Sorelli, Jessy Frech-Baronet, Julien Sanahuja, Matthieu Vandamme, Jeffrey Chen

Microindentation characterization and analytical modeling of the creep and relaxation behavior of a cement paste at different relative humidity

Zhao Chen[1], Luca Sorelli[2], Jessy Frech-Baronet[3], Julien Sanahuja[4], Matthieu Vandamme[5], Jeffrey Chen[6]

[1] Ph.D. student candidate, Dept. of Civil Engineering, Université Laval, Pavillon Adrien-Pouliot, 2940-Z, G1V 0A6, Canada. Email: zhao.chen.2@ulaval.ca

[2] Ph.D., Professor, Dept. of Civil Engineering, Université Laval, Pavillon Adrien-Pouliot, 2928-A, G1V 0A6 (corresponding author), Canada. Email: luca.sorelli@gci.ulaval.ca

[3] Ph.D. student candidate, Dept. of Civil Engineering, Université Laval, Pavillon Adrien-Pouliot, 2940-Z, G1V 0A6, Canada. Email: jessy.frech-baronet.1@ulaval.ca

[4] Ph.D., researcher, EDF R&D/MMC Department – Site des Renardiéres, Route de Sens, Ecuelles, F-77250 Moret sur Loing, France. Email: julien.sanahuja@edf.fr

[5] Ph.D., Assistant professor, Université Paris-Est, Laboratoire Navier, (UMR 8205), ENPC, CNRS, IFSTTAR, 77420 Champs-sur-Marne, France. Email: matthieu.vandamme@enpc.fr

[6] Ph.D., researcher, Lafarge Centre de Recherche, 38291 Saint Quentin Fallavier, France. Email: jeffrey.chen@lafargeholcim.com

Abstract

Recent studies have showed that microindentation techniques allow assessing the logarithmic creep rate of a cement paste in good correlation with the long-term creep rates measured by compressive tests at macroscopic scale. After having applied microindentation techniques to characterize the effect of relative humidity (RH) on both the creep and relaxation behaviour of a cement paste, the objective of this work is to analyze the duality between creep and relaxation curves by means of the analytical models which are currently employed in open literature. First, large grids of creep and relaxation microindentation tests were carried out on a cement paste sample in hygral

equilibrium at different levels of RH. Thus, the results were modeled by a viscoelastic model by considering different creep functions (logarithmic and power-law) and corrective terms for initial plasticity under loading. The presented results provide new insights to understand the duality between creep and relaxation rates of a cement paste measured at micrometer scale, especially considering the possible plastic effect.

1. Introduction

A recent survey has revealed that current methods and national codes significantly underestimate the long-term deflection of concrete bridges at about 20 years, and called the attention to the importance to better characterize the long-term creep mechanisms (Bažant et al., 2011). Estimating the long-term creep (e.g. basic creep without water exchange) of a concrete structure from short-term tests is unavoidable and yet unsolved crux in civil engineering (Brooks and Neville, 1978). One of the reason of such difficulty is that it takes few years to distinctly observe the long-term creep rate for a concrete sample with size of a dozen of centimeters, which is due to the time needed to exhaust water exchanges and drying creep (Brooks and Neville, 1978; Troxell et al., 1958a).

From a phenomenological point of view, concrete creep is usually split into parts, such as, short term due to drying creep and long-term due to basic creep, i.e., without moisture exchange (Pickett, 1942; Wittmann and Roelfstra, 1980; Bažant and Yunping, 1994; Bazant et al., 1997a; Cagnon et al., 2015). The short-term creep is assumed to primarily depend on water movement, whereas the long-term creep on inelastic mechanisms occurring at the scale of the Calcium-Silicate-Hydrate (C-S-H) sheets (Benboudjema et al., 2001; Torrenti et al., 2014). Numerous and complex models have been developed to describe the creep mechanisms, such as: (i) microdiffusion of water molecules between the hindered adsorbed layers and the capillary pores (Bazant and Chern, 1985a; Powers, 1965); (ii) sliding of C-S-H sheets (Vandamme and Ulm, 2009; Sanahuja and Dormieux, 2010; Bažant, 1972), like a viscous flow in shear sites which

undergo to micro-prestress relaxation (Bazant et al., 1997a); (iii) gel rearrangement as a sort of secondary consolidation process (Jennings, 2004); (iv) micro-cracking locally induced by microdiffusion (Rossi et al., 2012).

From an experimental point of view, by means of triaxial loading tests on leached cement pastes, Bernard et al. (2003) showed that the creep deformation is mostly volumetric at short term, although it becomes deviatoric at long-term. However, a recent analysis of several creep data available in open literature on undamaged cement pastes indicates that the Poisson's ratio is rather constant under loading (Aili et al., 2015). At high stress levels, the creep deformation may become strongly nonlinear due to microcracking, especially when relatively rigid inclusions are employed (Neville, A. M., 2006; Neville, 1971; Rossi et al., 2012).

Among several parameters which affect concrete creep, relative humidity (RH) is considered to play a major role on concrete creep (Brooks and Neville, 1978; Tamtsia and Beaudoin, 2000; Vandamme et al., 2015, 2015). Comparing creep results available in open literature is then not straightforward due to the nonuniform and often uncertain hygral conditions (Bazant and Li, 2008). Troxell et al. (1958b) performed creep compressive tests on concrete cylinders of approximately 100 mm diameter over 30 years showing that, after the drying creep is exhausted in approximately 1 year, the long-term creep is rather logarithmic in time and independent of the RH at which the sample was stored before testing. In a landmark work, Brooks measured the creep and shrinkage of several concretes stored in dry (i.e., RH equal to 65%) and wet conditions for a period of 30 years at approximately 20°C (Brooks and Neville, 1978). Brooks observed a logarithmic creep rate at long-term which was significantly greater for the stored wet samples. Furthermore, the greater the water-to-cement ratio (i.e. the water amount in the pores), the greater the creep rate. To reduce the effect of the RH gradient on the creep results, Wittman et al. (1968) employed small samples of millimetre size. Based on their results, Bazant and Chern (1985b) proposed a parabolic relationship

between the basic creep and the relative humidity for which creep increases, when the water content increases. Furthermore, Alizadeh et al. (2015) tested the creep deflection of millimetre beams of synthetic C-S-H confirming the important role of the water content.

Nowadays, microindentation technique has emerged for measuring the creep properties of cement-based materials as it can significantly reduce the time scale for observing long-term creep phenomena (Němeček, 2009; Nguyen et al., 2014, 2013; Pourbeik et al., 2013). By considering several mix designs, Zhang et al. (2013) have proven that, the long-term creep (i.e., basic creep) rates measured by microindentation are fairly well correlated with the ones measured by macroscopic compressive tests after 30 years. Due to the short time needed to reach the hygral equilibrium, the micrometric volume probed by microindentation is likely at hygral equilibrium after one day (Bazant and Chern, 1985a; Frech-Baronet et al., 2017). Finally, Zhang (2014) recently showed that an RH increase can augment long-term creep rate of synthetic C-S-H by a factor of about 5 when the relative humidity level increases from 11% to 95%. The creep and relaxation behaviour of a cement paste was also characterized with similar results (Sorelli et al., 2015).

From a modeling standpoint, simplified models have been widely employed in open literature to model creep indentation tests, especially based logarithmic creep compliance functions (Alizadeh et al., 2010; Cheng et al., 2005; Jones and Grasley, 2011a; Vandamme and Ulm, 2006). Notably, Vandamme performed a parametric finite element analysis to provide corrected analytical formula accounting for the effect of initial plasticity which occurs during the loading phase of an indentation test on a cement paste (Vandamme et al., 2012).

After having characterized the effect of the relative humidity on the creep and relaxation behaviour of a cement paste by means of microindentation, this work aims at applying analytical models, which are currently employed in open literature (Alizadeh et al.,

2010; Jones and Grasley, 2011a; Vandamme and Ulm, 2009), with special emphasis on the plasticity effect affecting the mathematical duality between creep and relaxation.

2. Materials and methods

2.1. Materials

A cement paste made with ordinary Portland clinker (type I) with a water-to-cement ratio (w/c) of 0.6 was investigated. The samples were cast in cylinder molds of 100 and 150 mm diameters. To avoid bleeding, the samples were kept in constant and uniform rotating equipment. They were then cured in chamber with very fine mist-like fog (relative humidity close to 100%) for 28 days and then stored at 50 ± 5% RH for 2 months at the temperature of 23 ± 2 °C. By the tests on three samples, the compressive strength is 20.3 MPa at 28 days, Young's modulus is 9.8 GPa, the porosity is 0.34, and Poisson ratio is 0.25 (Frech-Baronet et al., 2017). The porosity of the cement paste was measured on two samples by mercury intrusion porosimetry (MIP). The average porosity was approximately 34%, with the porosity distribution showing a quite large capillary porosity in the pore diameter range from 50 to 250 nm as shown in Figure 1.

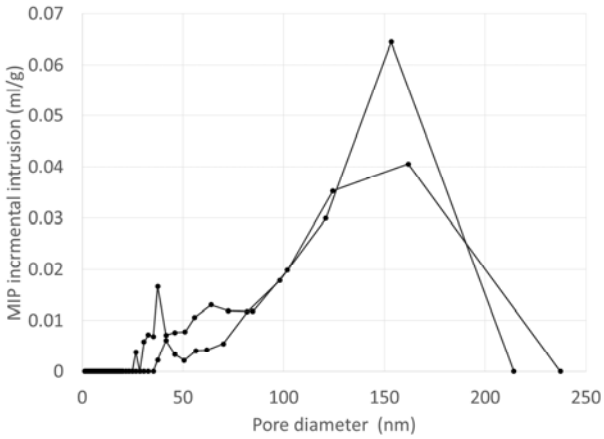

Figure 1. Two MIP measurements of the pore size distribution of the studied cement paste.

The cement paste was tested 90 days after casting to reduce the aging effect. Before testing, a cubic sample of 30 mm side was cut out from the center of the cylinder. By means of a digital microscope with a resolution of 0.1 μm, the indentation grid was located far from few observable defects (e.g. drying cracks, polishing cracks or large pores). A coarse grinding was performed using abrasive paper and water to smooth the edge of the samples. The surfaces were polished by 1 and 0.25 μm fineness diamond suspension oil-based solution. After polishing, the samples were put in an ultrasonic bath with isopropyl alcohol to remove particles left on the surface. The tests were performed on the same sample, which was sequentially stored at different RH from 33 ± 1% to 85 ± 1% with a curing time of 2 weeks at the testing of RH before microindentation testing. After each testing series, the sample was repolished completely removing any residual imprints within a depth of approximately 100 μm, and then cured again at the desired RH. Within a wide experimental campaign, no significant difference in creep and relaxation results was observed by increasing the RH curing from 1 to 7 days, suggesting that 1 day of RH curing is long enough to guarantee the hygral equilibrium of the micrometer zone probed by microindentation tests (Frech-Baronet et al., 2017).

2.2. Humidity chamber

As schematically shown in Figure 2 (a), a hermetic enclosure was built to control the RH, consisting of a closed circuit in which the hermetic enclosure was connected in series to an Erlenmeyer flask containing a solution of saturated salts and a pump (Sorelli et al., 2015). The use of a saturated salt solution (Table 1) was employed for reaching the specific humidity equilibrium. The hermetic system was endowed with a closed loop air circuit passing through the saturated salt solution. The RH and carbon dioxide (CO_2) concentration were continuously monitored by two sensors within the chamber. In this work, different levels of RH (33%, 55%, 75% and 85%) were considered. The concentration of CO_2 was reduced by adding an absorber in the hermetic room. For

security, the maximum value of RH was limited at 85% to avoid possible condensation in the chamber and damage to the electronical head of the microindenter.

Table 1. Solution used to control the relative humidity

Solution / water	RH at 20°C (%)	Solubility in water (g/100mL)
Magnesium Chloride ($MgCl_2$)	33.0± 0.3	54.3
Magnesium Nitrate $Mg(NO_3)_2$	55.0± 0.3	125.0
Potassium Chloride (KCl)	75.0± 0.3	34.4
Liquid water (H_2O)	85.0± 0.3	—

2.3. Surface roughness

The sample surface was carefully prepared for cement paste specimen according to an established protocol (Miller et al., 2008). As shown in Figure 2 (b), atomic force microscope (AFM) was employed to verify the surface topography of the cement paste. The roughness mean square (RMS), R_q, as calculated in (Miller et al., 2008) was about 65 nm as average on an area of approximately 50 μm × 50 μm, was far less than one-tenth of the indentation depth (4 μm), which indicates that the indentation surface was flat enough for properly measuring the indentation properties.

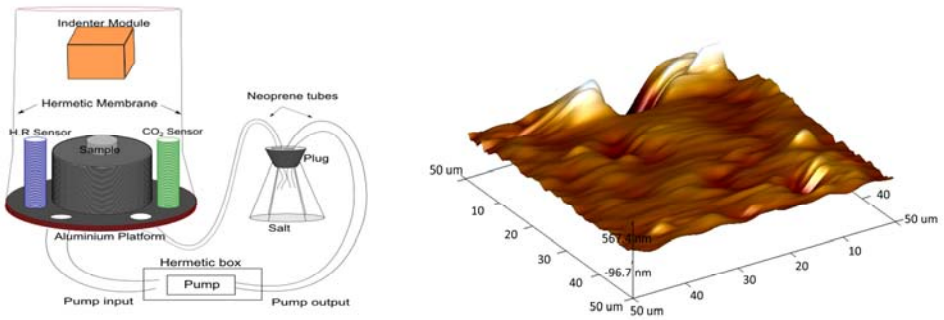

(a) (b)

Figure 2. (a) Hermetic chamber with humidity sensor and the CO_2 sensor connected in series to an air pump and an Erlenmeyer flask containing the solution of saturated salt; (b) AFM surface image of cement paste surface on an area of 50 μm × 50 μm (Frech-Baronet et al., 2017).

2.4. Basics of microindentation

Microindentation is a powerful technique to quantitatively measure the elasticity and hardness of cement paste hydrates (Nguyen et al., 2014, 2013; Pourbeik et al., 2013). During an indentation test, the force P and the penetration depth h are measured simultaneously, while the indenter tip penetrates into the film (Figure 3 (a)). A typical P-h curve (Figure 3 (b)) is constituted by a loading curve up to the maximum load P_{max}, followed by an unloading curve. The P-h curve is analyzed by extracting the indentation properties, such as: the indentation modulus $M = (S\sqrt{\pi}) / (2\beta A_c)$ and the indentation hardness $H = P_{max} / A_c$. The coefficient β accounts for the non-symmetrical shape of the indenter. The projected area A_c of the indenter-sample contact depends on the contact depth h_c (Figure 3 (a)). The contact stiffness $S = dP / dh$ is the slope measured during the initial stages of the unloading curve (Figure 3 (b)). The Young's modulus E of an isotropic material is estimated from the indentation modulus M as follows:

$M^{-1} = (1-\upsilon^2)/E + (1-\upsilon_i^2)/E_i$, where E_i and υ_i are the elastic modulus and the Poisson's ratio of the diamond tip, which are equal to 1141 GPa and 0.07, respectively; whereas E and υ are the Young modulus and the Poisson's ratio of the material, respectively.

Figure 3 (c) shows an experiment in which the load is linearly applied over time τ_L, then held constant over time τ_H, and finally reduced to zero over time τ_U. Although plastic deformation occurs during loading in a localized area underneath the indenter tip (Fischer-Cripps, 2004), it is generally assumed that the unloading curve is elastic, if the unloading is rather quick. As for a creep microindentation test, the asymptotic creep behavior ($t \to \infty$) can be characterized by the contact creep modulus C proposed by Vandamme and Ulm (2009), which describes the logarithmic asymptote of the creep penetration depth, as follows:

$$C \overset{def}{=} \lim_{t\to\infty} \frac{1}{t\,\dot{L}(t)} = \lim_{t\to\infty} \frac{P_{\max}}{2ta_U\,\dot{h}} = \frac{P_{\max}}{2a_U x_1} \tag{1}$$

where the indentation compliance $L(t)$ is such that its Carson transform is the inverse of Carson transform of the indentation relaxation modulus $M(t)$; x_1 = term of the logarithmic penetration depth function $\Delta h(t) = x_1 \ln(t/\tau_{ch} + 1)$ which is employed to fit the creep curve of the holding phase. This definition assumes that the radius of the contact area at unloading a_U is constant during holding, as experimentally verified with an error of approximately 5% (Vandamme, 2008a).

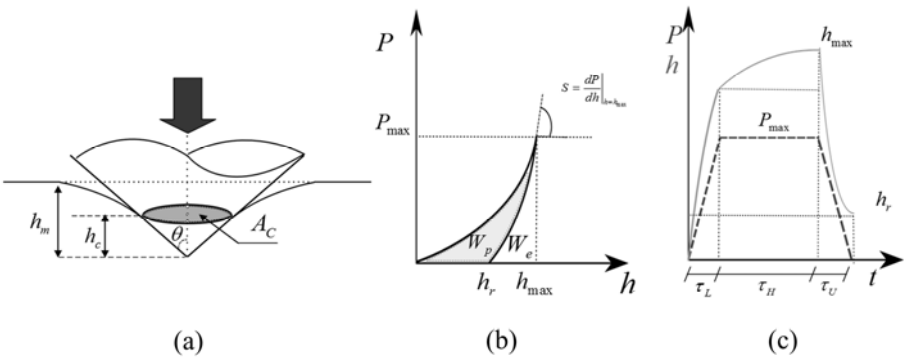

Figure 3. (a) Schematic view of an indentation test with a conical indenter; (b) Load versus penetration depth response; (c) Load and displacement vs. time.

2.5. Microindentation tests

The microindentation tests were carried out with the Anton-Paar Tritrec SA model microindentation Tester MHT^3. For this study, a Berkovich type diamond tip was employed, which is a three-sided pyramid with an equivalent cone semiangle θ of 70.3º. The micro-indenter tip was calibrated on a certified fused silica by fitting the data of contact area A_C versus h_c using the expression $A_C(h_c) = C_0 h_c^2 + C_1 h_c + C_2 h_c^{1/2} + C_3 h_c^{1/4} + \cdots$, where C_i are the fitting parameters (Oliver and Pharr, 1992). A grid of 10 by 10 microindentation tests with interdistance of 500 μm were performed on the cement paste for each RH under both test conditions, i.e., creep and relaxation. The loading setting for creep (or relaxation) tests were chosen as follows: (1) loading phase by imposing a constant load rate to achieve the maximum load P_{max} (or a constant speed to achieve the maximum h_{max}) in the loading time τ_L = 5 s; (2) the holding phase by imposing a constant load P_{max} (or a constant penetration depth h_{max}) for the holding time τ_H = 300 s; and (3) the unloading phase by imposing a constant unloading rate to remove P_{max} (or a constant speed to release the penetration depth) in the unloading time τ_U = 5 s. In a creep (or relaxation) test, the load (or the displacement) is controlled, while the penetration depth (or the load) is measured. The maximum load P_{max} = 8 N for creep testing was chosen

to be comparable to the maximum penetration depth h_{max} = 40 μm of relaxation testing. In accordance to previous studies, the loading time was rapid and much shorter than the holding time ($\tau_L << \tau_H$), so that viscous deformations can be neglected during the loading phase (Vandamme and Ulm, 2009).

The volume probed by microindentation has a size equal to five times the penetration depth h_{max} ((Vandamme et al., 2012), which results in a volume of approximately 8 million μm^3. Thus, as assumed in previous studies (Jones and Grasley, 2011a; Nguyen et al., 2014, 2013; Sorelli et al., 2015; Zhang, 2014), the cement paste volume probed by microindentation is considered large enough to yield a homogenous mechanical response. Figure 4 shows some typical imprints of microindentation tests observed by digital microscope at resolution of 0.1 mm. No microcracks greater than 0.1 μm were detected around the indentation imprints with a size of approximately 200 μm. Furthermore, possible abnormal values, which are likely due to surface defects, are not considered in the analysis (Constantinides, 2006; Krakowiak et al., 2015; Sorelli et al., 2008), Figure 5 shows an example of the spatial distribution of the microindentation properties (H and M) for the 10 x 10 indents as carried out in this study. With exception of a few abnormal high values, which were less than 5% of the total points, the indentation properties M and H exhibited a distribution with a coefficient of variation (COV) of approximately 11% and 19%, respectively (Table 2 and Table 3). Full details of the experimental results and analysis of variance (ANOVA) with effect of the loading

time, duration of RH curing, and the load level can be found in (Frech-Baronet et al., 2017).

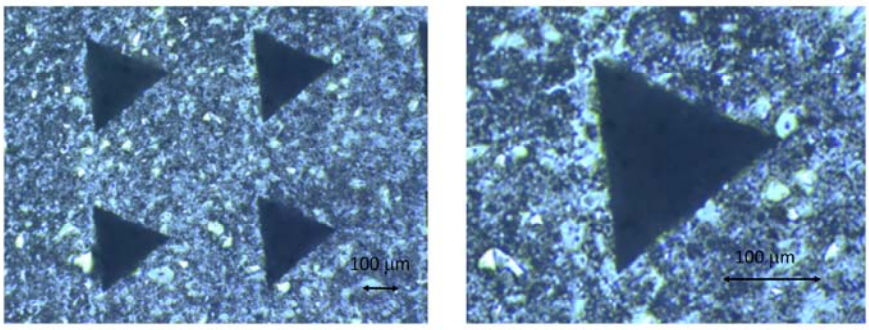

(a) (b)

Figure 4. View of the indentation imprints at different magnification by digital microscope (the length scale of 100 µm).

2.6. Viscoelastic analysis

The closed linear elastic solution between the penetration force P and the penetration depth h for an indenter tip with a conical shape was developed by Sneddon by a series of Hankel transforms (Sneddon, 1965) as follows:

$$h^2(t) = \frac{\pi P(t)}{2M \tan\theta} \tag{2}$$

where θ = half angle of a conical indenter tip. In the hypothesis of a purely linear viscoelastic solid (i.e., subjected to no plasticity), the viscoelastic solution of the indentation process can be obtained by the correspondence principle established by Sneddon as explained in (Vandamme, 2008a):

$$P(t) = \frac{2\tan\theta}{\pi}\int_0^t M(t-\xi)\frac{d}{d\xi}h^2(\xi)\,\mathrm{d}\,\xi \tag{3}$$

Considering the Laplace transform, i.e. $\widehat{f(s)} = \int_0^\infty e^{-st} f(t)dt$, the previous equation reads

$$\widehat{P(s)} = \frac{2\tan\theta}{\pi}\widehat{M(s)}s\widehat{h^2(s)} \tag{4}$$

The integral form of constitutive equations of isotropic viscoelastic material are written as (Findley et al., 1976):

$$\sigma(t) = \int_0^t E(t-\xi)\frac{\partial\varepsilon(\xi)}{\partial\xi}d\xi \tag{5}$$

$$\varepsilon(t) = \int_0^t J(t-\xi)\frac{\partial\sigma(\xi)}{\partial\xi}d\xi \tag{6}$$

where $\sigma(t)$ and $\varepsilon(t)$ are the uniaxial stress and strain. The function $E(t)$ and $J(t)$ are defined as the uniaxial relaxation modulus and creep compliance, respectively. Applying Laplace transform to these equations

$$\widehat{\sigma(s)} = s\widehat{E(s)}\widehat{\varepsilon(s)} \tag{7}$$

$$\widehat{\varepsilon(s)} = s\widehat{J(s)}\widehat{\sigma(s)} \tag{8}$$

Then the relation between the relaxation modulus $\widehat{E(s)}$ and the creep compliance $\widehat{J(s)}$ in Laplace domain

$$\widehat{E(s)} = \frac{1}{s^2\widehat{J(s)}} \tag{9}$$

The relation between the plane stress modulus $\widehat{M(s)}$ and the Poisson's ratio $\widehat{\nu(s)}$ in Laplace domain is (Jones and Grasley, 2011a)

$$s\widehat{M(s)} = \frac{s\widehat{E(s)}}{1-(s\widehat{\nu(s)})^2} \tag{10}$$

Based on a recent analysis of several creep data, Aili et al. (2015) observed that the coefficient Poisson's ratio (CPR) remains approximately constant or slightly decreases with time. A recent three-dimensional loading on cement paste seems to confirm that the CPR can be considered as constant (Grasley and Lange, 2007). Furthermore, Jones and Grasley (2011a) employed a constant CPR for analyzing the viscoelastic response of cement paste by nanoindentation. Therefore, the hypothesis of constant $\nu = 0.25$

holds for both the creep and the relaxation microindentation. In Laplace domain

$$\widehat{\nu(s)} = \frac{\nu}{s} = \frac{0.25}{s} \tag{11}$$

Consider the expression of $\nu(t)$ by the bulk modulus $K(t)$ and the shear modulus $G(t)$

$$s\widehat{\nu(s)} = \frac{3s\widehat{K(s)} - 2s\widehat{G(s)}}{6s\widehat{K(s)} + 2s\widehat{G(s)}} = 0.25 \quad \Rightarrow \quad \widehat{G(s)} = 0.6\widehat{K(s)} \tag{12}$$

which indicates that, under the assumption of constant CPR, relaxation bulk modulus $K(t)$ and shear modulus $G(t)$ are proportional to each other. From Equation (10) and Equation (11), the following equation can be readily obtained:

$$\widehat{M(s)} = \frac{\widehat{E(s)}}{1-\nu^2} \tag{13}$$

As the ratio of $\tau_L / \tau_H = 1/60$ is very small, the applied load can be assumed to be applied instantaneously as a Heaviside function (Jones and Grasley, 2011a; Vandamme, 2008a). For creep testing, $P(t) = P_{\max} H(t)$, and for relaxation testing, $h^2(t) = h^2_{\max} H(t)$. In Laplace domain

$$\widehat{P(s)} = \frac{P_{\max}}{s}, \quad \widehat{h^2(s)} = \frac{h^2_{\max}}{s} \tag{14}$$

With Equation (9), Equation (13) and Equation (14), Equation (4) is rewritten for the creep testing

$$\widehat{h^2(s)} = \frac{\pi P_{\max}(1-\nu^2)}{2\tan\theta}\widehat{J(s)} \tag{15}$$

With Equations (9), (13) (14), one can rearrange Equation (4) for the relaxation testing as follows:

$$\widehat{P(s)} = \frac{2\tan\theta h^2_{\max}}{\pi(1-\nu^2)}\widehat{E(s)} \tag{16}$$

where the $\widehat{E(s)} = 1/(s^2\widehat{J(s)})$. Inverting Equation (15) and Equation (16) into time domain, the following time dependent penetration depth $h(t)$ during creep and

penetration force $P(t)$ during relaxation are derived

$$h(t) = \sqrt{\frac{\pi P_{\max}(1-\nu^2)}{2\tan\theta} J(t)} \tag{17}$$

$$P(t) = \frac{2\tan\theta h_{\max}^2}{\pi(1-\nu^2)} E(t) \tag{18}$$

Those relations are valid only if the indentation was purely linear viscoelastic, i.e., no plasticity. Although, the visco-elastic analysis is widely employed by other researchers in modeling nanoindentation creep results (Grasley and Lange, 2007; Nguyen et al., 2014, 2013), it can be considered as a first-order solution because plastic phenomena are unavoidable when using a sharp tip occur during the loading phase (Vandamme et al., 2012).

2.7. Plastic effect

Undoubtedly, the cement paste below a Berkovich tip is subjected to complex plastic deformation during the loading. Based on a numerical validation with a finite element analysis, Vandamme et al. (2012) proposed to correct the viscoelastic Equation (17) and Equation (18) for considering the effect of plasticity occurring during loading, as follows:

$$\dot{L(t)} = \frac{2a_U \dot{h(t)}}{P_{\max}} \tag{19}$$

$$\frac{M(t)}{M_0} = \frac{P(t)}{P_{\max}^t} \tag{20}$$

where $L(t)$ = contact creep compliance; $M(t)$ = contact relaxation modulus; M_0 = indentation modulus of the material; $P_{\max}^t$ = recorded maximum load of the relaxation testing. By performing the integration on both sides of Equation (19), the following equation is derived:

$$L(t)-L(0)=\frac{2a_U}{P_{\max}}[h(t)-h(0)]=\frac{2a_U\Delta h(t)}{P_{\max}} \tag{21}$$

where $L(0)=1/M_0=(1-\upsilon^2)/E_0$, E_0 is the elastic modulus of the cement paste, and Δh(t) is the increase of depth during holding. With the relation of $\widehat{L(s)}$ and $\widehat{M(s)}$ in Laplace domain

$$\widehat{L(s)}=\frac{1}{s^2\widehat{M(s)}} \tag{22}$$

In conjunction with Equation (9) and Equation (13), the contact creep compliance can be rewritten as

$$\widehat{L(s)}=\frac{1-\upsilon^2}{s^2\widehat{E(s)}}=(1-\upsilon^2)\widehat{J(s)} \tag{23}$$

which is the relation between the contact creep compliance $\widehat{L(s)}$ and the uniaxial creep compliance $\widehat{J(s)}$ in the Laplace domain. Inverting Equation (23) into the time domain and combining it with Equation (21)

$$(1-\upsilon^2)[J(t)-\frac{1}{E_0}]=\frac{2a_U\Delta h(t)}{P_{\max}} \tag{24}$$

With Equation (13) and $M_0=E_0/(1-\upsilon^2)$, the expression of the relaxation is given by

$$\frac{\widehat{M(s)}}{M_0}=\frac{\widehat{E(s)}}{E_0} \tag{25}$$

Inverting Equation (25) into the time domain and combining it with Equation (20)

$$\frac{E(t)}{E_0}=\frac{P(t)}{P_{\max}^t} \tag{26}$$

Like Equations (17) and (18), Equations (24) and (26) make it possible to link creep and relaxation data to meaningful viscous material properties, but independent of whether plasticity occurred during loading.

2.8. Logarithmic creep compliance

Based on several observations at different length scales, concrete creep appears to be well captured by a logarithmic function in the long-term (Bazant et al., 1997b; Torrenti et al., 2014; Vandamme, 2008a). Therefore, the following well-established logarithmic creep compliance is adopted from Vandamme (2008a)

$$J(t)-J(0)=\frac{1}{E_{v1}}\ln\left(1+\frac{t}{\tau_1}\right) \tag{27}$$

where $J(0)=1/E_i\,(i=0,\ 1)$ = creep compliance function at the end loading time: E_0 = elastic modulus of cement paste for Equations (24) and (26), E_1 = fitting parameter controls the elastic-plastic penetration of the instantaneous loading phase for Equations (17) and (18); the modulus E_{v1} and the characteristic time τ_1 control the magnitude and the shape of creep during the holding phase, respectively. Applying the Laplace transform to Equation (27) (Bateman, 1954), the authors obtain

$$\widehat{J(s)}-\frac{J(0)}{s}=\frac{e^{s\tau_1}Ei(s\tau_1)}{E_{v1}s} \tag{28}$$

where $Ei(x)$ = exponential integral with non zero value of x given by

$$Ei(x)=-\int_{-x}^{\infty}\frac{e^{-t}}{t}dt \tag{29}$$

Thus the relaxation modulus in Laplace domain reads

$$\widehat{E(s)}=\frac{E_{v1}}{[J(0)E_{v1}+e^{s\tau_1}Ei(s\tau_1)]s} \tag{30}$$

Equation Equation (30) cannot be analytically transformed into the time domain with Laplace transform tables. But it can be inverted numerically with the Gaver-Stehfest formula (Abate 2006), which is

$$\widehat{f}\left(t,\overline{M}\right)=\frac{\ln(2)}{t}\sum_{k=1}^{2\overline{M}}\zeta_k\,\widehat{f}\left(\frac{k\ln(2)}{t}\right)$$
$$\zeta_k=(-1)^{\overline{M}+k}\sum_{j=\lfloor(k+1)/2\rfloor}^{k\wedge\overline{M}}\frac{j^{\overline{M}+1}}{\overline{M}!}\binom{\overline{M}}{j}\binom{2j}{j}\binom{j}{k-j} \tag{31}$$

where $\overline{M}$ = positive integer that controls the precision of the inversed numerical function; $\lfloor(k+1)/2\rfloor$ = greatest integer less than or equal to $(k+1)/2$, and $k\wedge\overline{M}=\min(k,\overline{M})$. As for the relaxation modeling, $\overline{M}$ of Gaver-Stehfest formula was set as 8 to keep the precision of the numerical inversion. The numerical algorithm was implemented in an algorithm in Maple within a least squares fitting method.

2.9. Power-law creep compliance

To check if possible mismatch between model and experiment depends on the particular choice of the creep compliance function, a power creep function is also considered (Bažant and Osman, 1976). The creep compliance of the power-law model is written as (Aigner et al., 2009)

$$J(t)-J(0)=\frac{1}{E_{v2}}\left(\frac{t}{\tau_2}\right)^k \tag{32}$$

where the modulus E_{v2} controls the magnitude during the holding phase; the characteristic time τ_2 and the index k control the shape of the holding phase. In the Laplace domain, Equation (32) reads (Bateman, 1954)

$$\widehat{J(s)-\frac{J(0)}{s}}=\frac{1}{E_{v2}}\frac{1}{\tau_2^k s^{k+1}}\Gamma(k+1) \tag{33}$$

where $\Gamma(x)$ is the gamma function with definition

$$\Gamma(x)=\int_0^\infty t^{x-1}e^{-t}dt \tag{34}$$

The relaxation modulus is given by

$$\widehat{E(s)}=\frac{1}{s^2\widehat{J(s)}}=\frac{E_{v2}\tau_2^k s^{k-1}}{J(0)E_{v2}\tau_2^k s^k+\Gamma(k+1)} \tag{35}$$

which can be numerically inverted into the time domain with Equation (31).

3. Results and discussion

Figure 5 shows an example of indentation grid for the cement paste tested at 33% RH with the mapping of the indentation modulus and hardness. Interestingly, the cement paste is slightly stiffer and harder at a lower relative humidity, as previously obtained by Zhang (2014). Figure 6 (a and b) show the experimental mean curves for the creep tests (*h*-*t*) and for the relaxation tests (*P*-*t*) only for the holding phase, respectively, at the considered levels of RH. The time and the penetration depth or load are shifted to zero, i.e., zero time starts from the onset of the holding phase. The effect of the RH on the experimental mean creep and relaxation curves is evident.

The microindentation results for the creep and relaxation tests at the various RHs are summarized in Table 2 and Table 3, including the COVs (which represent the average value over the entire holding time for the mean curve's penetration depth versus time, h-t, or load versus time, P-t) and the standard deviation of the measurements (reported by indicating the mean value ± standard deviation). The COVs were less than 10%, which indicates a standard deviation of approximately 0.3-0.5 μm. A variation of humidity from 33 to 85% causes a reduction of the contact creep modulus C by a factor of 2.4 (i.e., the long-term creep rate increases).

Table 2. Results of creep testing.

RH	*CV*	Indentation modulus	Hardness	h_{max}	a_U	*C*
(%)	(%)	(GPa)	(MPa)	(μm)	(μm)	(GPa)
33	9.9	14.5 ± 1.1	220.0 ± 31.0	40.5 ± 2.9	111.2	136.3
55	5.0	14.1 ± 2.2	224.0 ± 55.0	41.2 ± 6.9	111.8	95.7
75	6.0	12.1 ± 1.7	175.0 ± 38.0	46.0 ± 6.1	124.6	65.5
85	7.5	13.3 ± 1.1	177.0 ± 29.0	45.1 ± 4.2	122.0	57.2

Table 3. Results of relaxation testing.

RH	*CV*	Indentation modulus	Hardness	P_{max}
(%)	(%)	(GPa)	(MPa)	(N)
33	6.8	15.4 ± 1.4	192.0 ± 39.0	6.9 ± 1.3
55	4.4	14.6 ± 2.3	181.0 ± 60.0	6.5 ± 2.1
75	7.1	14.0 ± 1.6	152.0 ± 29.0	5.5 ± 1.1
85	8.6	13.1 ± 1.0	135.0 ± 20.0	4.9 ± 0.7

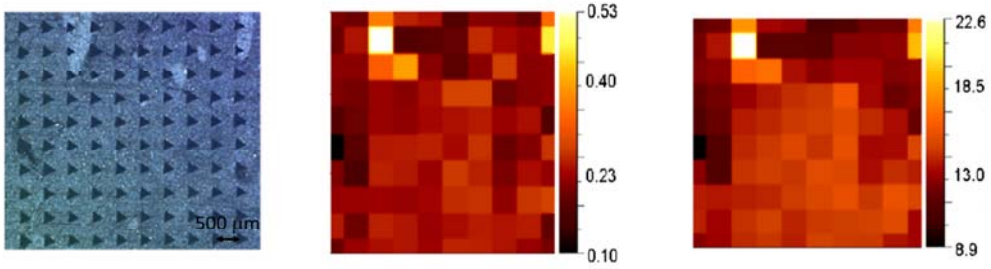

Figure 5. (a) Example of indentation grid on the cement paste for RH=33%; (b) mapping of the indentation hardness (GPa); (c) mapping of the indentation modulus (GPa) (Frech-Baronet et al., 2017).

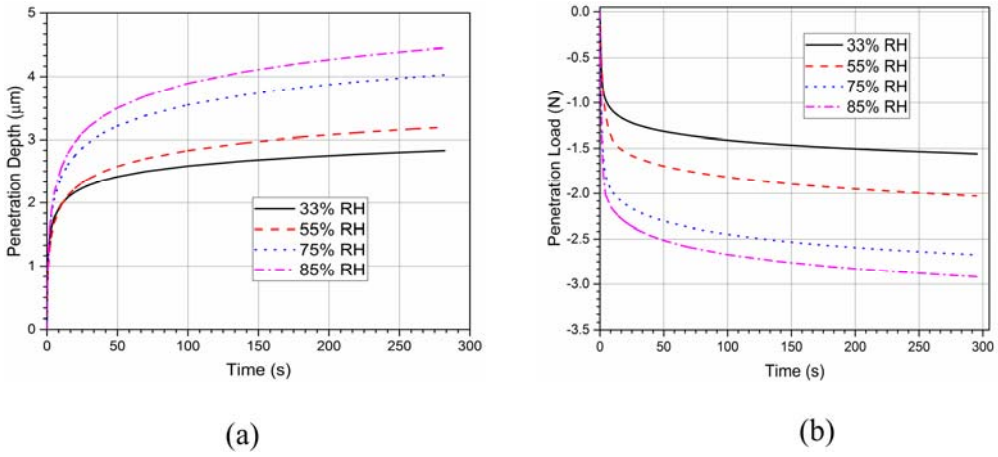

(a) (b)

Figure 6. (a) Creep tests: penetration depth vs. time during the holding phase; (b) Relaxation tests: applied load vs. time during the holding phase.

3.1. Viscoelastic modeling

Firstly, the overall creep and relaxation curves were separately best fitted by means of the viscoelastic model based on logarithmic or power-low function. Figure 7 (a and b) show the comparison between the experimental and simulated results for the creep and the relaxation tests by making use of the previously discussed logarithmic compliance with Equation (27) and power-law compliance with Equation (32) within the viscoelastic model with Equations (17) and (18). Notably, when fitted on the relaxation data, the creep functions were inverted with the numerical scheme as described in Equation (31). The fitted parameters are summarized in Table 4 and Table 5. Considering the residual error, the logarithmic model seems to fit better the entire experimental creep or relaxation curves. Figure 7 (a and b) show the comparison between the experimental results and the simulated ones for the creep and the relaxation tests, respectively, with logarithmic and power-law compliance.

Passing from an RH of 33 to 85%, the creep compliance modulus E_{v1} and E_{v2} reduces by a factor of 2.2 and 9.2, respectively, for the logarithmic creep compliance; although they reduce by a factor of 1.1 and 2.1, respectively, for the power-law creep compliance. Finally, Figure 8 (a and b) compare the creep and relaxation parameters (E_{v1}, τ_1 or E_{v2}, τ_2) in function of the relative humidity for the logarithmic and power compliance. Unfortunately, the model parameters best fit over the entire curves are rather different in the case of relaxation or creep tests, no matter the choice of the creep functions (E_{v1}, τ_1 for the logarithmic creep compliance, or E_{v2}, τ_2 for the power-law creep compliance).

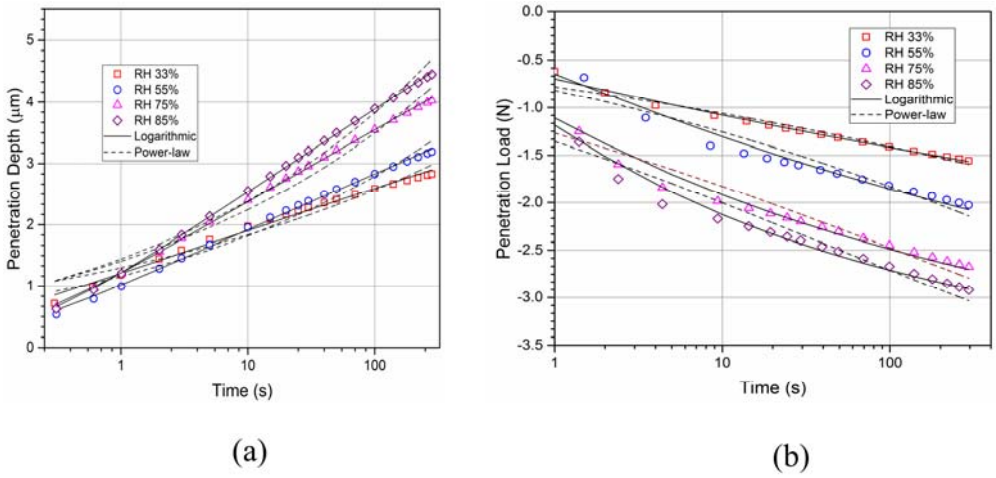

Figure 7. Viscoelastic analysis: Comparison between the experimental and simulated results for the (a) creep tests; (b) relaxation tests.

Table 4. Viscoelastic analysis: best fitting parameters with logarithmic creep function.

	RH	E_1	E_{v1}	τ_1	Residual
	(%)	(GPa)	(GPa)	(s)	
Creep	33	2.57	164.88	0.020	0.064 μm^2
	55	2.48	121.84	0.091	0.021 μm^2
	75	1.99	84.04	0.115	0.014 μm^2
	85	2.07	73.92	0.161	0.0076 μm^2
Relaxation	33	2.27	70.86	0.0323	0.0095 N^2
	55	2.15	32.98	0.209	0.096 N^2
	75	1.82	14.11	0.171	0.140 N^2
	85	1.63	7.73	0.304	0.120 N^2

Table 5. Viscoelastic analysis: best fitting parameters with power law creep function.

	RH	E_1	E_{v2}	τ_2	k	Residual
	(%)	(GPa)	(GPa)	(s)	-	
Creep	33	2.58	45.40	0.244	0.144	0.387 μm^2
	55	2.50	53.41	0.158	0.179	0.502 μm^2
	75	2.00	39.07	0.181	0.187	0.714 μm^2
	85	2.09	43.18	0.098	0.197	0.893 μm^2
Relaxation	33	2.30	24.04	0.0614	0.141	0.0385 N^2
	55	2.18	25.93	0.0326	0.198	0.389 N^2
	75	1.86	12.78	0.0189	0.205	0.551 N^2
	85	1.66	11.25	0.0143	0.241	0.609 N^2

3.2. Viscoelastoplastic modeling

Analogously to the previous analysis, the overall creep and relaxation curves were separately best fitted by means of the viscoelastoplastic model of Equations (24) and (26). When fitted on the relaxation data, the creep functions are processed with the numerical scheme described in Equation (31). The best-fitted parameters with least square method are summarized in Table 6 and Table 7. Figure 9 (a and b) show the comparison between the experimental results and the simulated ones for the creep and the relaxation tests, respectively, with logarithmic (27) and power-law compliance (32).

Considering the rate of the creep compliance of the logarithmic model in Equation (27), the characteristic time τ_1 controls the initial creep rate, but it has no influence on the long-term creep rate as also shown in Table 6. Indeed, the rate of creep compliance can be rewritten as $\dot{J}(t) \approx 1/(E_{v1}t)$ for large times. Passing from an RH of 33 to 85%, the creep compliance modulus E_{v1} and E_{v2} reduces by a factor of 2.2 and 7.7, respectively, for the logarithmic creep compliance, whereas they reduce with a factor of 1.2 and 1.9, respectively, for the power-law compliance.

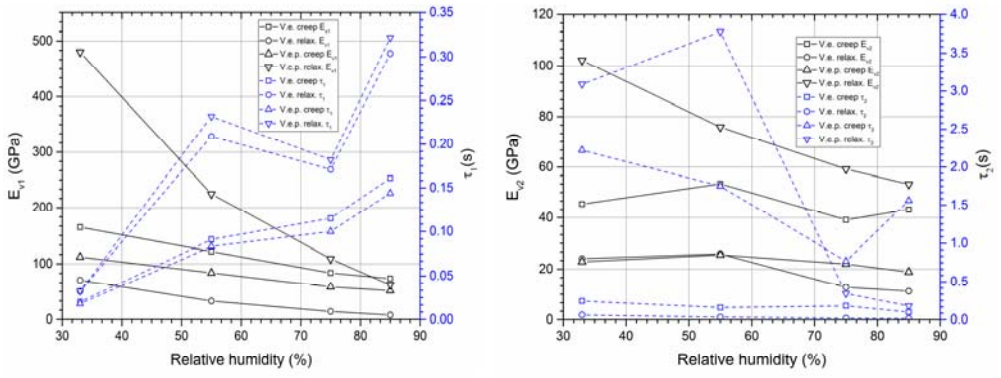

(a) (b)

Figure 8. (a) Comparison in term of creep compliance parameters (E_{v1} and τ_1 or E_{v2} and τ_2) versus RH for the viscoelastic and viscoelastoplastic model based on (a) the logarithmic creep compliance; (b) power-law creep compliance.

Figure 8 (a and b) compare the creep and relaxation parameters (E_{v1}, τ_1 or E_{v2}, τ_2) in function of the relative humidity for the logarithmic and power-law compliance. However, the best fitting parameters are still rather different in the case of relaxation and creep tests. For instance, in the case of logarithmic compliance function, the parameter E_{v1} for creep is close to that of the relaxation ($E_{v1,creep}$=83% $E_{v1,relaxation}$), but for lower RH their mismatch increases ($E_{v1,creep}$=23% $E_{v1,relaxation}$). A similar mismatch is observed on the parameters fitted with the power-law model (32) of the creep function (see Table 7). Interestingly, the characteristic time increases when the relative humidity increases for both the models based on the logarithmic creep compliance functions (Figure 8 (a)), but it decreases when the relative humidity increases for the viscoelastoplastic model based a power-law power function (Figure 8 (b)).

This mismatch of the model parameters for creep and relaxation tests can be mainly explained by the following reasons: (1) the delayed plasticity, which may occur during the holding phase of a creep test, is not considered by Equations (24) and (26) as suggested by Vandamme (2008a); (2) the fact that the duration of the loading is finite, which is neglected in the analysis, may play a role; and (3) possibly, an additional

mechanism may be at stake during creep tests at constant loading, e.g., micro-cracking (Mazzotti and Savoia, 2002; Rossi et al., 2012).

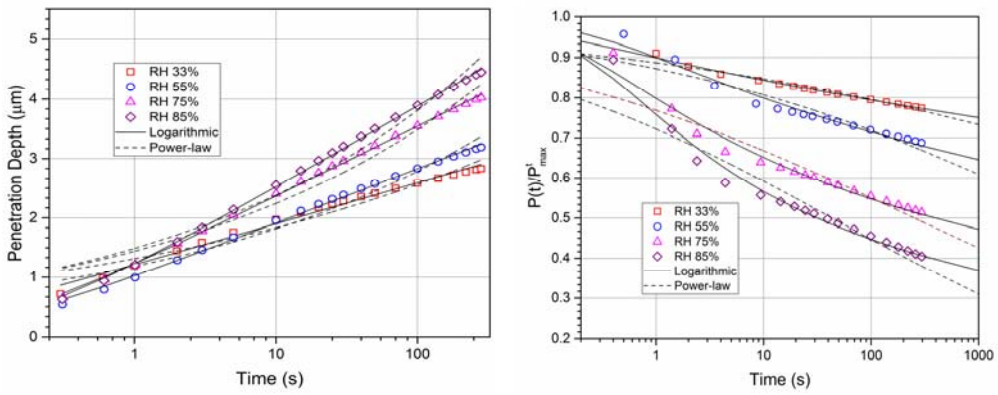

Figure 9. Viscoelastoplastic analysis: comparison between the experimental and simulated results for the creep tests (a) and relaxation tests (b).

Table 6. Viscoelastoplastic analysis: best fitting parameters for logarithmic model.

	RH	E_{v1}	τ_1	Residual
	(%)	(GPa)	(s)	
Creep	33	112.2	0.0179	0.073 μm^2
	55	84.1	0.0833	0.029 μm^2
	75	58.7	0.100	0.023 μm^2
	85	51.8	0.144	0.017 μm^2
Relaxation	33	480.4	0.0325	0.0095 N^2
	55	224.8	0.232	0.098 N^2
	75	109.0	0.182	0.14 N^2
	85	62.7	0.322	0.12 N^2

Table 7. Viscoelastoplastic analysis: best fitting parameters for power-law model.

	RH	E_{v2}	τ_2	k	Residual
	(%)	(GPa)	(s)	-	
Creep	33	22.88	2.22	0.145	0.41 μm^2
	55	25.52	1.75	0.186	0.55 μm^2
	75	21.98	0.768	0.192	0.81 μm^2
	85	18.87	1.56	0.204	1.04 μm^2
Relaxation	33	102.22	3.09	0.151	0.044 N^2
	55	75.87	3.78	0.211	0.41 N^2
	75	59.16	0.343	0.214	0.57 N^2
	85	53.24	0.180	0.248	0.63 N^2

In summary, the RH reduces the creep compliance parameter E_{v1}, i.e., to increase the viscous deformations for creep or relaxation experiments. Furthermore, for the viscoelastic analysis, the values of E_{v1} estimated for the creep tests are much greater than those ones estimated from the relaxation tests. Instead, accounting for the plasticity during initial loading caused a reduction of the compliance values E_{v1} estimated on creep tests and an increase of E_{v1} estimated on relaxation tests. Interestingly, the values of E_{v1} for creep tests showed a difference of 16% with respect to the creep compliance modulus C (Table 2).

3.3. Modeling long-term creep and relaxation rates

Finally, a final analysis was carried out for calculating the optimal model parameters which can simultaneously best fit the experimental long-term slopes of creep and relaxation curves at the end of the holding time (~300 seconds), which was estimated over the last 10 s. In accordance to previous works (Jones and Grasley, 2011; Vandamme, 2008; Zhang et al., 2013), the expression *long-term* indicates that the

holding time (~ 300 seconds) is much greater than the characteristic time τ_1. The optimization was performed by minimizing the errors between experimental slopes and simulated ones simultaneously for creep and relaxation curves with a least squares fitting approach. For the viscoelastoplastic model with logarithmic creep compliance function, it was possible to find a unique set of model parameters (E_{v1}, τ_1) which best fit both the creep and relaxation experimental long-term rates. The experimental and simulated slopes at the end of the holding phase are presented in Table 8, whereas the corresponding model parameters are summarized in Table 9.

Table 8. Comparison of the experimental and simulated slopes at the end of the holding phase for both creep and relaxation tests.

	Experimental slope		Optimized slope		Error	
RH (%)	Creep ($\times10^{-3}$μm/s)	Relaxation ($\times10^{-3}$N/s)	Creep ($\times10^{-3}$μm/s)	Relaxation ($\times10^{-3}$N/s)	%	
33	0.775	-0.578	0.767	-0.573	1.0	0.9
55	1.274	-0.753	1.274	-0.753	0.0	0.0
75	1.593	-0.767	1.583	-0.770	0.6	0.4
85	1.955	-0.845	1.946	-0.852	0.5	0.8

Table 9. Optimized model parameters fitting the slopes at the end of the holding phase for both creep and relaxation tests.

RH (%)	E_{v1} (GPa)	τ_1 (s)
33	160	0.006
55	95	0.14
75	69	0.60
85	57	2.10

The minimized errors between the experimental and simulated long-term rate for both creep and relaxation is less than 1%. This confirms that increasing RH from 33% to 85%

reduces the creep compliance modulus E_{v1} with a factor of approximately 2.8 confirming, i.e., the water content favors long-term rate of both creep and relaxation of a cement paste (Alizadeh et al., 2010; Brooks and Neville, 1978; Ruetz, 1968; Sorelli et al., 2015; Troxell et al., 1958b; Wittmann, 1970; Q. Zhang et al., 2013). The E_{v1} parameter is now very close to the contact creep compliance C with a difference of 5%. Remarkably, the creep compliance modulus C can be suitably employed to predict the long-time rates for both creep and relaxation, which are related by the mathematical transformations of Equation (31).

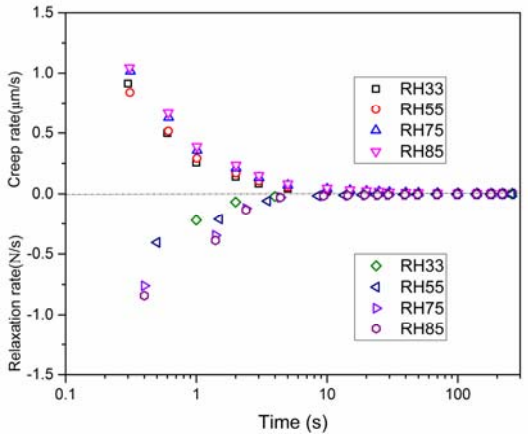

Figure 10. Creep and relaxation rate measured experimentally on cement paste by microindentation tests at various levels of RH.

Finally, Figure 10 shows the experimental creep and relaxation rate in function of time in semilog graph, indicating a certain convergence after approximately 10 s. This confirms that, beyond such a short period when delayed plasticity may occur, the proposed viscoelastic model based on logarithmic creep function best fits the long-term behaviour. If such delayed plasticity is due to a damage mechanism, the cracks should be of sub-micrometer size as no visible microcracks were detected by digital microscope observations (Figure 4).

4. Conclusion and outlook

Based on an analytical modeling of a wide experimental campaign of creep and relaxation microindentation tests on a cement paste with a w/c of 0.6, the following conclusions are drawn:

- The elastic indentation modulus M and the indentation hardness H slightly increased by reducing the RH from 85 to 33%. This slight strengthening and stiffening is perhaps due to the increase of the internal suction in large capillary pores, as a sort of poromechanical effect. More important, the experimental contact creep modulus C reduces from 136 GPa to 57 GPa, suggesting that moisture content increases the ability of the C-S-H to creep;
- The logarithmic creep compliance seems relatively more accurate than the power-law compliance for fitting the *entire* experimental curve of the creep or relaxation microindentation curves;
- From a mathematical point of view, the numerical method based on Laplace transform and the Gaver-Stehfest algorithm was presented, which allows calculation of the relaxation indentation response from the creep compliance function;
- From a modeling point of view, starting from a corrective formula validated against a finite element analysis (Vandamme et al., 2012), an approximated viscoelastoplastic solution which accounts for the occurrence of plasticity during loading has been proposed for both creep and relaxation tests;
- The viscoelastoplastic model allowed for simulating the experimental long-term rates of both creep and relaxation microindentation tests by means of a unique logarithmic creep compliance function. Increasing RH from 33 to 85% reduced the creep compliance modulus E_{v1} by a factor of approximately 3;
- During a creep microindentation test, delayed viscoplasticity may occur in the first 10 s of the holding phase. However, cracks with a size greater than a

micrometer were not observed around the indentation imprints. The relaxation response during microindentation tests seem to provide a viscoelastic response that is not affected by the effect of delayed plasticity. Beyond the initial time of approximately 10 seconds, both creep and relaxation microindentation tests provide results which can be coherently predicted by a logarithmic creep compliance function;

- The logarithmic creep compliance modulus E_{v1} is eventually similar to the contact creep modulus C, which can therefore be suitably employed to predict the long-term rates of both creep and relaxation microindentation tests.

As an outlook, there is a need of further research for modeling the entire creep and relaxation microindentation response. For example, by better accounting for the plasticity effects with numerical models and by developing physically based creep compliance functions that consider different mechanisms acting at short-term and long-term points during an indentation test (e.g., water movement and C-S-H sliding).

Acknowledgements

Authors would like to thank NSERC Discovery programme with grant No. 386488 and the China Scholarship Council (CSC) for supporting funding to the Ph.D. students and laboratory expenses.

References

Aigner, E., Lackner, R., Pichler, C., 2009. Multiscale prediction of viscoelastic properties of asphalt concrete. J. Mater. Civ. Eng. 21, 771–780.

Aili, A., Vandamme, M., Torrenti, J.-M., Masson, B., 2015. Theoretical and practical differences between creep and relaxation Poisson's ratios in linear viscoelasticity. Mech. Time-Depend. Mater. 19, 537–555.

Alizadeh, R., Beaudoin, J.J., Raki, L., 2010. Viscoelastic nature of calcium silicate

hydrate. Cem. Concr. Compos. 32, 369–376.

Bateman, H., 1954. Tables of integral transforms. Calif. Inst. Technol. Bateman Manuscr. Proj. N. Y. McGraw-Hill 1954 Ed. Erdelyi Arthur 1.

Bažant, Z., 1972. Thermodynamics of interacting continua with surfaces and creep analysis of concrete structures. Nucl. Eng. Des. 20, 477–505.

Bazant, Z.P., Chern, J.C., 1985a. Concrete creep at variable humidity: constitutive law and mechanism. Mater. Struct. 18, 1–20.

Bazant, Z.P., Chern, J.C., 1985b. Concrete creep at variable humidity: constitutive law and mechanism. Mater. Struct. 18, 1–20.

Bazant, Z.P., Hauggaard, A.B., Baweja, S., Ulm, F.-J., 1997a. Microprestress-solidification theory for concrete creep. I: Aging and drying effects. J. Eng. Mech. 123, 1188–1194.

Bazant, Z.P., Hauggaard, A.B., Baweja, S., Ulm, F.-J., 1997b. Microprestress-solidification theory for concrete creep. I: Aging and drying effects. J. Eng. Mech. 123, 1188–1194.

Bažant, Z.P., Hubler, M.H., Yu, Q., 2011. Excessive creep deflections: An awakening. Concr. Int. 33, 44–46.

Bazant, Z.P., Li, G.-H., 2008. Comprehensive database on concrete creep and shrinkage. ACI Mater. J. 105, 635–637.

Bažant, Z.P., Osman, E., 1976. Double power law for basic creep of concrete. Matér. Constr. 9, 3–11.

Bažant, Z.P., Yunping, X.I., 1994. Drying creep of concrete: constitutive model and new experiments separating its mechanisms. Mater. Struct. 27, 3–14.

Benboudjema, F., Meftah, F., Sellier, A., Heinfling, G., Torrenti, J.M., 2001. A basic creep model for concrete subjected to multiaxial loads., in: Fourth International Conference on Fracture Mechanics of Concrete and Concrete Structures. pp. 161–168.

Bernard, O., Ulm, F.-J., Germaine, J.T., 2003. Volume and deviator creep of calcium-leached cement-based materials. Cem. Concr. Res. 33, 1127–1136.

Brooks, J.J., Neville, A.M., 1978. Predicting long-term creep and shrinkage from short-term tests. Mag. Concr. Res. 30, 51–61.

Cagnon, H., Vidal, T., Sellier, A., Bourbon, X., Camps, G., 2015. Drying creep in cyclic humidity conditions. Cem. Concr. Res. 76, 91–97.

Cheng, L., Xia, X., Scriven, L.E., Gerberich, W.W., 2005. Spherical-tip indentation of viscoelastic material. Mech. Mater. 37, 213–226.

Constantinides, G., 2006. Invariant mechanical properties of calcium-silicate-hydrates (CHS) in cement-based materials: instrumented nanoindentation and microporomechanical modeling. Massachusetts Institute of Technology.

Findley, W.N., Lai, J.S., Onaran, K., 1976. Nonlinear Creep and Relaxation of Viscoelastic Materials, With an Introduction to Linear Viscoelasticity. North-Holland, Amsterdam.

Fischer-Cripps, A.C., 2004. Nanoindentation Springer. N. Y.

Frech-Baronet, J., Sorelli, L., Charron, J.-P., 2017. New evidences on the effect of the internal relative humidity on the creep and relaxation behaviour of a cement paste by micro-indentation techniques. Cem. Concr. Res. 91, 39–51.

Grasley, Z.C., Lange, D.A., 2007. The viscoelastic response of cement paste to three-dimensional loading. Mech. Time-Depend. Mater. 11, 27–46.

Jennings, H.M., 2004. Colloid model of C− S− H and implications to the problem of creep and shrinkage. Mater. Struct. 37, 59–70.

Jones, C.A., Grasley, Z.C., 2011a. Short-term creep of cement paste during nanoindentation. Cem. Concr. Compos. 33, 12–18.

Jones, C.A., Grasley, Z.C., 2011b. Short-term creep of cement paste during nanoindentation. Cem. Concr. Compos. 33, 12–18.

Krakowiak, K.J., Wilson, W., James, S., Musso, S., Ulm, F.-J., 2015. Inference of the

phase-to-mechanical property link via coupled X-ray spectrometry and indentation analysis: Application to cement-based materials. Cem. Concr. Res. 67, 271–285.

Mazzotti, C., Savoia, M., 2002. Nonlinear creep, Poisson's ratio, and creep-damage interaction of concrete in compression. ACI Mater. J. 99, 450–457.

Miller, M., Bobko, C., Vandamme, M., Ulm, F.-J., 2008. Surface roughness criteria for cement paste nanoindentation. Cem. Concr. Res. 38, 467–476.

Němeček, J., 2009. Creep effects in nanoindentation of hydrated phases of cement pastes. Mater. Charact. 60, 1028–1034.

Neville, A. M., 2006. Properties of Concrete, 4th edition. ed. Pearson Education.

Neville, A.M., 1971. Creep of concrete: plain, reinforced, and prestressed.

Nguyen, D.-T., Alizadeh, R., Beaudoin, J.J., Pourbeik, P., Raki, L., 2014. Microindentation creep of monophasic calcium–silicate–hydrates. Cem. Concr. Compos. 48, 118–126.

Nguyen, D.-T., Alizadeh, R., Beaudoin, J.J., Raki, L., 2013. Microindentation creep of secondary hydrated cement phases and C–S–H. Mater. Struct. 46, 1519–1525.

Oliver, W.C., Pharr, G.M., 1992. An improved technique for determining hardness and elastic modulus using load and displacement sensing indentation experiments. J. Mater. Res. 7, 1564–1583.

Pickett, G., 1942. The effect of change in moisture-content on the crepe of concrete under a sustained load, in: Journal Proceedings. pp. 333–356.

Pourbeik, P., Alizadeh, R., Beaudoin, J.J., Nguyen, D.-T., Raki, L., 2013. Microindentation creep of 45 year old hydrated Portland cement paste. Adv. Cem. Res. 25, 301–306.

Powers, T.C., 1965. Mechanism of shrinkage and reversible creep of hardened cement paste. Struct. Concr. Its Behav. Load 319–344.

Rossi, P., Tailhan, J.-L., Le Maou, F., Gaillet, L., Martin, E., 2012. Basic creep behavior

of concretes investigation of the physical mechanisms by using acoustic emission. Cem. Concr. Res. 42, 61–73.

Ruetz, W., 1968. A hypothesis for the creep of hardened cement paste and the influence of simultaneous shrinkage. Proc. Struct. Concr. Its Behav. Load 365–387.

Sanahuja, J., Dormieux, L., 2010. Creep of a CSH gel: a micromechanical approach. An. Acad. Bras. Ciênc. 82, 25–41.

Sneddon, I.N., 1965. The relation between load and penetration in the axisymmetric Boussinesq problem for a punch of arbitrary profile. Int. J. Eng. Sci. 3, 47–57.

Sorelli, L., Constantinides, G., Ulm, F.-J., Toutlemonde, F., 2008. The nano-mechanical signature of ultra high performance concrete by statistical nanoindentation techniques. Cem. Concr. Res. 38, 1447–1456.

Sorelli, L., Frech-Baronet, J., Charron, J.P., 2015. Creep Behavior of Cement Paste, Mortar, and Concrete: The Role of Relative Humidity and Interface Porosity. Presented at the Concreep 10, Wien, pp. 296–304.

Tamtsia, B.T., Beaudoin, J.J., 2000. Basic creep of hardened cement paste a re-examination of the role of water. Cem. Concr. Res. 30, 1465–1475.

Torrenti, J.M., Benboudjema, F., Barré, F., Gallitre, E., 2014. On the very long term delayed behaviour of concrete, in: Proceedings of the International Conference on Ageing of Materials & Structures.

Troxell, G.E., Raphael, J.M., Davis, R.E., 1958a. Long-time creep and shrinkage tests of plain and reinforced concrete, in: ASTM Proceedings. pp. 1–20.

Troxell, G.E., Raphael, J.M., Davis, R.E., 1958b. Long-time creep and shrinkage tests of plain and reinforced concrete, in: ASTM Proceedings. pp. 1–20.

Vandamme, M., 2008a. The nanogranular origin of concrete creep: a nanoindentation investigation of microstructure and fundamental properties of calcium-silicate-hydrates. Massachusetts Institute of Technology.

Vandamme, M., 2008b. The nanogranular origin of concrete creep: a nanoindentation

investigation of microstructure and fundamental properties of calcium-silicate-hydrates. Massachusetts Institute of Technology.

Vandamme, M., Bažant, Z.P., Keten, S., 2015. Numerical Study of the Creep of Slit Nanopores: Role of Water, in: 10th International Conference on Mechanics and Physics of Creep, Shrinkage, and Durability of Concrete and Concrete Structures.

Vandamme, M., Tweedie, C.A., Constantinides, G., Ulm, F.-J., Van Vliet, K.J., 2012. Quantifying plasticity-independent creep compliance and relaxation of viscoelastoplastic materials under contact loading. J. Mater. Res. 27, 302–312.

Vandamme, M., Ulm, F.-J., 2009. Nanogranular origin of concrete creep. Proc. Natl. Acad. Sci. 106, 10552–10557.

Vandamme, M., Ulm, F.-J., 2006. Viscoelastic solutions for conical indentation. Int. J. Solids Struct. 43, 3142–3165.

Wittmann, F., 1970. Einfluss des Feuchtigkeitsgehaltes auf das Kriechen des Zementsteines. Rheol. Acta 9, 282–287.

Wittmann, F., 1968. Surface tension skrinkage and strength of hardened cement paste. Matér. Constr. 1, 547–552.

Wittmann, F.H., Roelfstra, P.E., 1980. Total deformation of loaded drying concrete. Cem. Concr. Res. 10, 601–610.

Zhang, Q., 2014. Creep properties of cementitious materials: effect of water and microstructure: An approach by microindentation. Université Paris-Est.

Zhang, Q., Le Roy, R., Vandamme, M., Zuber, B., 2013. Long-term creep properties of cementitious materials-Comparing compression tests on concrete with microindentation tests on cement, in: Poromechanics V@ SProceedings of the Fifth Biot Conference on Poromechanics. ASCE, pp. 1596–1604.

Zhang, Q, Le Roy, R., Vandamme, M., Zuber, B., 2013. Long-term creep properties of cementitious materials–comparing compression tests on concrete with

microindentation tests on cement. Presented at the American Society of Civil Engineers, pp. 1596–1604.